Journal of Materials Science: Materials in Electronics (2019) 30:2600–2609
https://doi.org/10.1007/s10854-018-0535-6

Enhancement in electrochemical performance of nitrogen-doped hierarchical porous carbon-based supercapacitor by optimizing activation temperature

Lin Tang[1] · Yibei Zhou[1] · Xinyi Zhou[1] · Yuru Chai[1] · Qiaoji Zheng[1] · Dunmin Lin[1]

Received: 5 August 2018 / Accepted: 10 December 2018 / Published online: 11 December 2018

Abstract
The electrochemical performance of carbon-based supercapacitor is closely related with the microscopic characteristics of electrode materials. Here, nitrogen-doped hierarchical porous carbons (NHPC) was fabricated by KOH treatment and pyrolyzation using pig nail as a protein-rich biomass source, and microscopic characteristics of the materials were effectively tailored by optimizing activation temperature to enhance electrochemical performance of carbonaceous materials for supercapacitor. The results show that the optimum activation temperature is 800 °C. The constructed NHPC-800 displays three-dimensional interconnected honeycomb structure, possesses high specific surface area (2563.30 $m^2\ g^{-1}$) with high-speed ion transfer channels. Additionally, NHPC-800 deliver superior capacitance with 251.4 F g^{-1} at 1 A g^{-1}. Besides, a remarkable energy density of 29.43 Wh kg^{-1} corresponding to power density of 847.9 W kg^{-1} is verified by an assembled symmetric supercapacitor in $EMIMBF_4$ electrolyte.

1 Introduction

Recently, environment issue has become extremely urgent and noticeable. In addition, the shortage of renewable energy resources also hinders sustainable development of human society. Hence, looking for new energy storage and conversion devices has become an immediate requirement [1–3]. Lithium ion battery has made great revolution in the past few years. However, relatively low power density limits its charge/discharge rate during electrochemical reaction process [4]. Supercapacitor, as well named electrochemical capacitor or ultracapacitor, has attracted extensive attention owing to its remarkable power density (~ 10,000 W kg^{-1}), rapid charge/discharging rate (charging/discharging quickly in a short time), long cycle life (> 100,000 cycles), low operation and maintenance cost as well as high safety factor [5]. Hence, supercapacitor has great potential to become next generation energy storage device for potential applications of universal electronic equipment. Although supercapacitor possesses a great number of advantages, relatively low energy density is the great barrier for its practical application in modern/next-generation electronic back-ups [6, 7]. Therefore, the current development goal of supercapacitor is to further increase its energy density.

Generally speaking, electrochemical performance of supercapacitor principally relies on electrode materials. Hence, developing novel electrode materials is an effective technique to promote property of supercapacitor. In recent years, supercapacitor electrode materials include metal oxides, conductive polymers as well as carbonaceous materials [8–10]. Although metal oxide such as ruthenium dioxide exhibits excellent electrochemical properties, high cost and poor conductivity limit its widespread application. In addition, conducting polymers are frequently confronted with the obstacle of poor cycling stability, which imputes to irreversible swell and shrink of volume during electrochemical reaction process [11–13]. Recently, carbons (e.g. graphene [14], carbon nanotubes [15], porous carbon [16]) have aroused considerable attention owing to their abundant reserves, low cost, superior conductivity and high chemical stability [17–20]. Nevertheless, graphene and carbon nanotube have some shortcomings of high-cost, complex preparation process, non-renewable precursors and highly corrosive reagents, which impede their large-scale applications [21]. Among various carbon materials, porous carbon has attracted intense attention on account of its large specific

✉ Dunmin Lin
ddmd222@sicnu.edu.cn

[1] College of Chemistry and Materials Science, Sichuan Normal University, Chengdu 610066, China

surface area (SSA), remarkable conductivity, prominent stability, low price and eco-friendliness, which can act as a promising candidate of supercapacitor [22]. Although SSA is a vital factor to electrochemical performance for porous carbon materials, specific capacitance does not linearly increase with SSA because of wide pore size distribution of porous carbon including micropores, mesopores and macropores. Tiny micropores (< 0.3 nm) are identified to be inaccessible to electrolyte ions, severely degenerating electrochemical property of porous carbon [23]. Compared with microporous carbon, ordered mesoporous carbons (OMCs) can provide sufficient ion transmission channel and demonstrate a more superior electrochemical property [24]. Nevertheless, relatively low SSA (~ 1000 m^2 g^{-1}) and porosity of large mesopores still impedes capacitance of OMCs. Hence, suitable pore size is crucial for enhancing capacitance of porous carbon. There are three prerequisite ingredient for porous carbons of supercapacitors: high SSA, outstanding electro-conductivity, as well as admirable electrolyte accessibility to internal porosity of carbon matrix. From the above, a hierarchical pore morphology with coexistence of micro-, meso-, and macropores can effectively improve electrochemical property of supercapacitor [25]. For hierarchical porous carbon, adequate micropores and mesopores can supply sufficient accessible SSA, which can generate high specific capacitance and energy density. Besides, abundant mesopores and macropores can promote ion transfer into internal space of carbon matrix, guaranteeing excellent rate capacitance and power density. In addition, heteroatoms doping also acts crucial roles in enhancing electrochemical property of carbon-based materials [26]. Nitrogen doping can not only improve surface wettability on of carbon, but also generate extra faradaic pseudocapacitance, which are beneficial to ion diffusion of supercapacitors [27–29]. Despite of enormous achievements for heteroatom-doped porous carbon, complicated preparation process, costly precursor and poisonous by-product are not favor of its large-scale production and utilization [30, 31]. Recently, biomass carbons and their derivatives can act as alternatives for heteroatom-doped porous carbons with large SSA and multistage pore morphology owing to their natural abundance, easy accessibility, low cost and environment friendliness [32–34]. Biomass-derived porous carbon materials (human hair [35], pigskin [36], wheat flour [37], coconut shell [38]) by a simple preparation process exhibit excellent energy density and power density.

Pig nail usually is abandoned as a common waste during food production process. The primary ingredient of pig nail is scleroprotein, including α-helix keratins and β-lamella keratins. Furthermore, more than 7.35 million tons pig nails were produced every year. Due to its increasing volume in global region, appropriate managements of pig nail have become a worldwide issue. Considering a great deal of nitrogen content in pig nail, it is viable to convert it into nitrogen-rich carbonaceous materials for application in supercapacitors. This technique could meet the urgent requirement for both disposal of pig nail and manufacture of carbonaceous material. The obtained porous material at the activation temperature of 800 °C possesses 3D honeycomb interconnected network and large SSA, which are advantageous to ion transport and storage in the process of charging/discharging and thus exhibits outstanding capacitance performance, rate performance and cycle stability.

2 Experimental

2.1 NHPC preparation

Pig nail was gathered from Chengdu supermarket. Pig nails were first washed several times with deionized water until there is no impurity and finally dried at 100 °C for 6 h. Dried pig nails were pre-carbonized in a tuber furnace at 300 °C and then heated for 2 h on N_2 flow. Then pre-treatment materials were thoroughly mixed with KOH (AR) in mass ratio of 2:1. Subsequently, mixture was stirred to form an uniform liquid and heated to the high temperature (700 °C, 800 °C and 900 °C, respectively) with rate of 2 °C min^{-1} and kept for 1 h at N_2 atmosphere. Obtained products were adequately washed using 1 M HCl (AR) and deionized water until pH 7. Specimens were named as NHPC-*x, x* being activation temperature of 700, 800 and 900, respectively.

2.2 Material characterizations

Scanning electron microscope (SEM) was displayed on JSM-7500 SEM (Japan). X-ray diffractometer (XRD, Smart Lab, Rigaku, Japan) and Raman spectrometer (Renishaw RM2000, UK) was performed to identify crystallographic structure of specimens. Transmission electron microscope (TEM) was characterized on GZF20 (USA). The SSA was detected via nitrogen adsorption–desorption isotherms (Micromeritics ASAP2020, USA) and counted by Brunauer Emmett Teller (BET) method. X-ray photoelectron spectroscopy (XPS) was measured on XPS spectrometer (Thermo ESCALAB 250XI, USA) to investigate the composition and valence state of surface elements of samples. Thermogravimetric analysis (DSC-TGA, Q500, American) was performed at air atmosphere up to 800 °C.

2.3 Electrochemical characterization

To fabricate working electrode in three-electrode system, 80 wt% NHPC-*x*, 10 wt% acetylene black and 10 wt% PVDF was mixed in *N*-methylpyrrolidone (NMP). The Hg/HgO electrode was employed as the reference electrode,

while a platinum gauze electrode was served as counter electrode. The electrochemical impedance spectroscopy (EIS), galvanostatic charge–discharge (GCD) and cyclic voltammetry (CV) were performed on the Shanghai CHI660E electrochemical workstation. The cycle performance test was recorded on CT2001A Land Battery Tester.

The specific capacitance was obtained via formula (1):

$$C = \frac{I \times \Delta t}{m \times \Delta V} \tag{1}$$

where C (F g^{-1}) is specific capacitance; I (A) is discharge current; Δt (s) is discharge time; m (g) is electroactive substance mass; and ΔV (V) refers to voltage change.

The electrochemical performances were also investigated in a NHPC-based symmetric supercapacitor. The symmetric capacitor was assembled into a 2032 cell, which was formed by two nearly identical electrodes, $EMIMBF_4$ electrolyte and glassy fibrous separator.

Energy and power densities of symmetric supercapacitor were defined by formulas (2) and (3):

$$E = \frac{C \times \Delta V^2}{2 \times 4 \times 3.6} \tag{2}$$

$$P = \frac{3600 \times E}{\Delta t} \tag{3}$$

where E (Wh kg^{-1}) and P (W kg^{-1}) are the energy density and power density; C (F g^{-1}) refers to specific capacitance; ΔV (V) is the voltage change during discharge process; and Δt (s) is the discharge time.

3 Results and discussion

3.1 Characterization

It can be seen that morphologies of NHPC-*x* gradually alter with the increasing in activation temperature(Fig. 1a–c). When activation temperature is 700 °C, NHPC-700 consists of a small number of macropores (Fig. 1a) and possesses the widest average distance between neighbor pores of all specimens. The microstructure of NHPC-700 may not be conducive to transfer of electrolyte ions. With activation temperature increasing to 800 °C, NHPC-800 exhibits more highly interlinked honeycomb-like pore structure (Fig. 1b), which is beneficial to transmission of ion/electron between electrolyte and electrode surface. However, pore structure of NHPC-900 suffers over corrosion due to excessive temperature (Fig. 1c). It can be seen that all materials show porous framework with numerous pores. The architectural feature with dense pore structure was ascribed to pyrolyzation of collagen and release of plentiful gaseous substances (such as carbonic oxide, carbon dioxide and hydrogen) [39]. Hence, the optimum activation temperature is 800 °C at which the obtained porous material possesses 3D honeycomb-like interconnected network. This 3D honeycomb-like structure with abundant porosity not only is highly beneficial to effective electrochemical contact of electroactive substance and electrolyte, but also assists permeation of electrolyte into interior of carbonaceous materials [40]. In addition, the mapping images imply the uniform distribution of C (Fig. 1e), N (Fig. 1f) and O (Fig. 1g) in NHPC-800. Furthermore, oxygen/nitrogen-containing functional groups

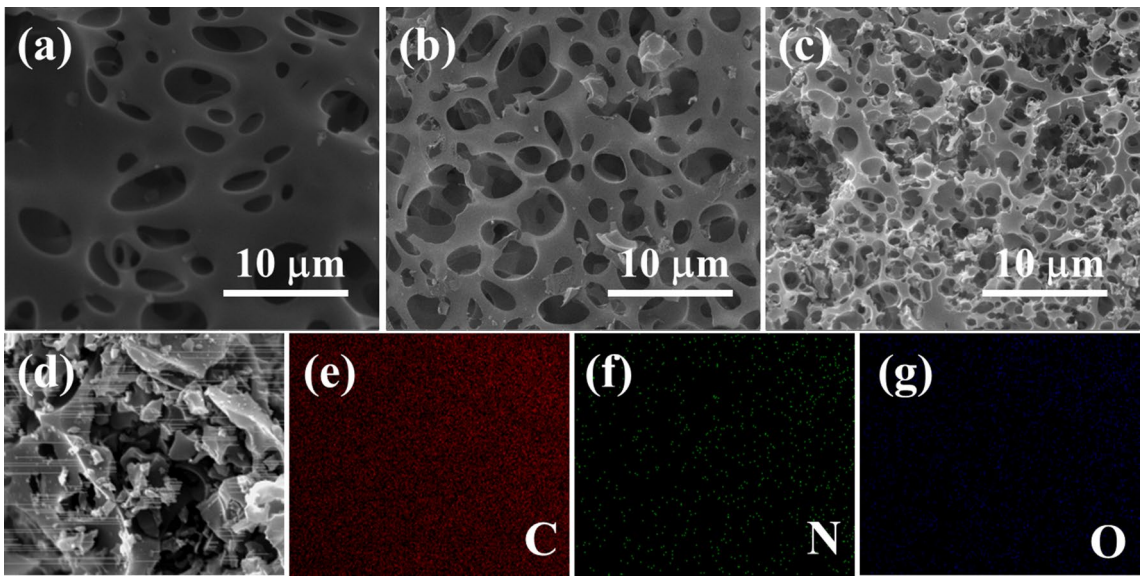

Fig. 1 SEM images of **a** NHPC-700, **b** NHPC-800 and **c** NHPC-900; elemental mappings **d**–**g** of NHPC-800

play vital roles in improving electrochemical performance of carbon materials [26, 41].

The TEM images of NHPC-800 at different magnifications are shown in Fig. 2a–d. Figure 2a displays cross-linked porous structure of NHPC-800. As shown in Fig. 2b, a rough nanostructure layer with mesopores and micropores can be clearly observed. With the improvement of magnification (Fig. 2c, d), abundant micropores can be also observed. These indicate that NHPC-800 possesses hierarchical porous structure. This unique morphology with coexistence of various sizes of pores primarily depends on chemistry activation at high temperature. The activation mechanism between carbon and KOH can be proceeded as: $6KOH + C \rightarrow 2K + 3H_2 + 2K_2CO_3$ [42, 43]. During reaction process, the generation of a large amount of gas (H_2, CO, CO_2) is favorable to form a great quantity of pores, which provide abundant store spaces and wide transmission paths for electrolyte ions.

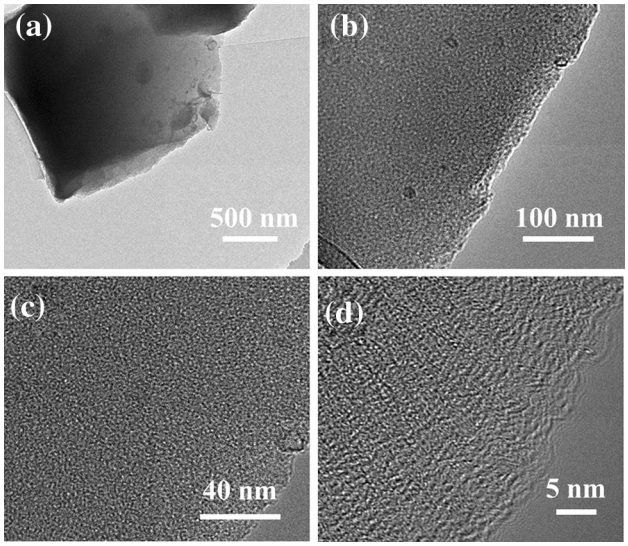

Fig. 2 TEM images of **a**–**d** NHPC-800

Figure 3 displays N_2 physisorption analyses of NHPC-*x*. From Fig. 3a, all samples exhibit typical I and IV isotherms, illustrating coexistence of micropores and mesopores in NHPC-*x* [44, 45]. As shown in Fig. 3b, pore sizes with $x = 700$, 800 and 900 centrally distribute at 0–3.5 nm. Table 1 exhibits porous characteristics of samples. Visibly, the porosity of NHPC-*x* is distinctly affected by activation temperature. The SSA and pore volume of NHPC-700 are 1394.24 $m^2\ g^{-1}$ and 0.73 $cm^3\ g^{-1}$, which are the lowest among all samples. As

Table 1 Pore parameters of samples

NHPC-*x*	S_{BET} [a] ($m^2\ g^{-1}$)	V_{total} [b] ($cm^3\ g^{-1}$)	V_{micro} [b] ($cm^3\ g^{-1}$)	V_{meso} [b] ($cm^3\ g^{-1}$)
NHPC-700	1394.24	0.73	0.46	0.27
NHPC-800	2563.30	1.35	0.51	0.84
NHPC-900	2370.37	1.26	0.33	0.92

[a]SSA obtained by Multi-Point BET method

[b]Total pore micropore and mesopore volume derived from density functional theory (DFT)

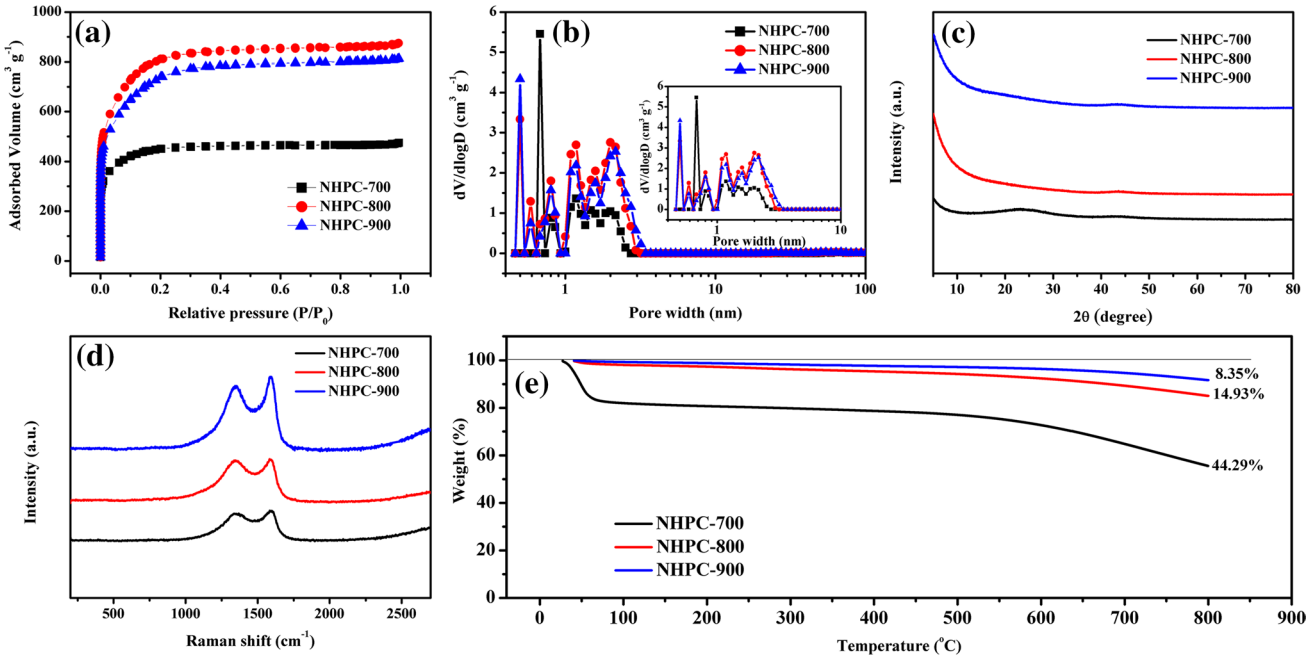

Fig. 3 **a** Nitrogen sorption isotherms; **b** pore size distributions; **c** XRD patterns; **d** raman spectras; and **e** TGA patterns of NHPC-*x*

activation temperature rising to 800 °C, the SSA prominently increases to 2563.30 $m^2 g^{-1}$, and pore volume also prominently enlarges to 1.35 $cm^3 g^{-1}$, which can be attributable to sufficient etching by KOH and adequate pyrolysis of collagen at high temperature. However, at high temperature of 900 °C, the SSA and pore volume of NHPC-900 reduce to 2370.37 $m^2 g^{-1}$ and 1.26 $cm^3 g^{-1}$, which ascribe to partial collapse of pore structure due to excessive temperature. It is worth noting that NHPC-800 possesses highest SSA and the most plentiful porosity with optimal hierarchical porous morphology, which can provide massive ion absorption sites and transmission channels and thus is conductive to rapid transfer of electrolyte ion [38]. XRD patterns of NHPC-*x* are displayed in Fig. 3c. NHPC-*x* have two broad diffraction peaks located at ~25° and 44°, corresponding to (002) and (101) planes, respectively [46]. The peak intensities of the NHPC-800 and NHPC-900 obviously become weaker compared to NHPC-700, illustrating distinct graphitization and crystallinity decrease due to the existence of amorphous carbon structure after activation by KOH [47]. Figure 3d shows the Raman spectras of the NHPC-*x*. Two characteristic peaks located at around 1340 cm^{-1} and 1590 cm^{-1} accord to D-band and G-band. It is well-known that D-band stands for structural defect, while the G-band is associated with the graphite degree of carbon materials [48]. The intensity ratio (I_D/I_G) can illustrate graphitization degree of carbonaceous sample [48]. Lower the I_D/I_G ratio is, greater the graphitization degree [28]. When the temperature increased from 700 to 900, the I_D/I_G values of samples are 0.71, 0.98 and 0.89, respectively. As the temperature rises from 700 to 800 °C, the I_D/I_G value increases from 0.71 to 0.98. Probably, a high activation temperature can lead to a higher amount of defects and disordered structures because of more chemical reaction between KOH and the graphitized area in the carbon particle [49]. It should be noted that the I_D/I_G value decreases from 0.98 to 0.89 with the temperature further increasing to 900 °C, which may be attributed to the partial collapse of pore structure and exposure of internal atomic structure due to excessive high temperature. The TGA curves of NHPC-*x* are revealed in Fig. 3e. The mass losses of NHPC-700, NHPC-800 and NHPC-900 are 44.29%, 14.93% and 8.35%, respectively, which indicate that the defects structures increase with the enhancing of pyrolysis temperature.

Chemical components of NHPC-800 have been analyzed via XPS (Fig. 4). Three distinct peaks of carbon (283.77 eV), nitrogen (399.25 eV) and oxygen (531.04 eV) element with their contents of 86.66, 2.10, 11.24 at.% are observed in Fig. 4a. C 1s located at 283.73, 284.71, 287.59 and 289.97 eV correspond to C–C, C–N, C–O and C=O, respectively (Fig. 4b). From Fig. 4c, the N 1s can be discovered to N-6 (398.54 eV, pyridinic N), N-5 (399.85 eV, pyrrolic N), N-Q (401.72 eV, quaternary N), N-X (402.63 eV, oxidized N), respectively [50, 51]. pyridinic and pyrrolic nitrogen are conducive to formation of defects at surface as well as edge of carbon materials and the increase in electrochemical reaction activity sites to trigger pseudocapacitance

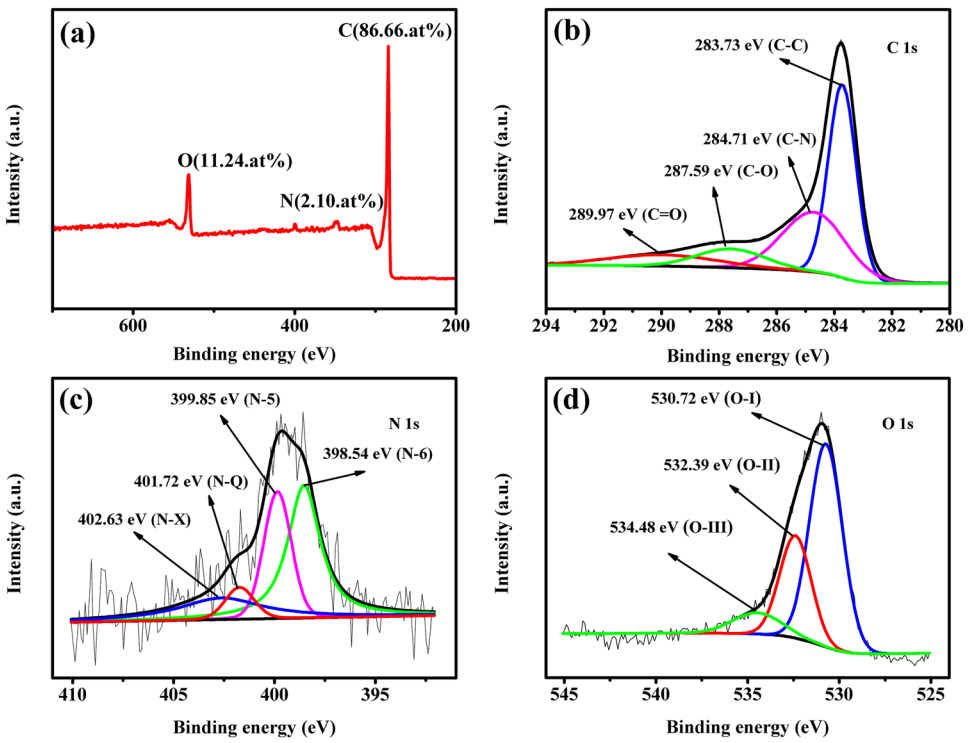

Fig. 4 **a** XPS spectra; and high-resolution XPS spectra analysis of NHPC-800: **b** C 1s; **c** N 1s; and **d** O 1s

behavior during the charging/discharging process [52]. Pyridinic and pyrrolic nitrogen can induce pseudocapacitance as following faradic process [53]:

$$> CH{-}NH_2 + 2OH^- \leftrightarrow > C{=}NH + 2H_2O + 2e^- \quad (4)$$

$$> C{-}NH_2 + 2OH^- \leftrightarrow > C{-}NHOH + H_2O + 2e^- \quad (5)$$

In addition, N–Q in the carbon skeleton can abate the resistance of charge migration to improve the electrical conductivity [21]. The O 1s depicted in Fig. 4d can be fitted into three peaks, including O-I (530.72 eV), O-II (532.39 eV), O-III (534.48 eV), respectively. It is generally believed that oxygen doping can also enhance electrochemical performance via introducing faradaic pseudocapacitance [41]. It is reported that nitrogen and oxygen doping have remarkable electron-donor feature and higher charge movability, which can induce electron donor properties, lessen work-function as well as provide high surface energy and surface reactivity in electron-transfer process, thus enhancing surface wettability of electrode material. This is favorable for increasing the contact area of electrolyte and electrode material [54, 55]. In summary, the introduction of heteroatom can increase the electrochemical performance of carbon electrode for supercapacitor [56, 57].

3.2 Electrochemical characterizations

The electrochemical performances of NHPC-*x* have been evaluated in a three-electrode system. With CV at 5 mV s^{-1}, all samples present approximately rectangular CV shapes (Fig. 5a), implying dominant electrical double-layer capacitor behavior. It is noticeable that NHPC-800 shows the maximum loop area among the three samples, indicating that NHPC-800 has the highest specific capacitance, which ascribe to its high SSA and interrelated honeycomb-like porous structure [58]. The GCD curves of samples are

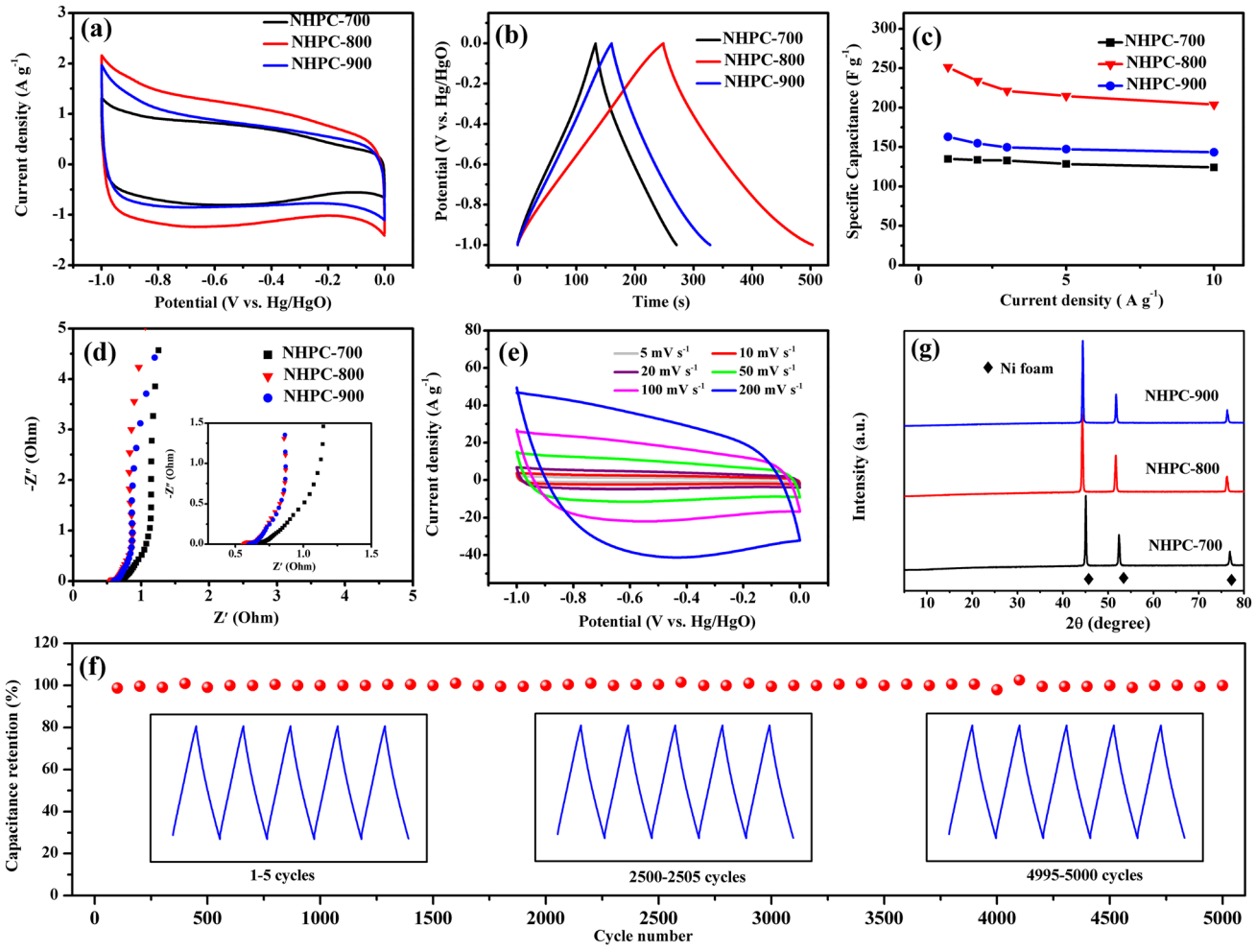

Fig. 5 Electrochemical property of NHPC-*x* in6 M KOH: **a** CV curves at 5 mV s^{-1}; **b** GCD curves at 1 A g^{-1}; **c** specific capacitances of NHPC-*x* at different current densities; **d** Nyquist plots; **e** CV curves of NHPC-800; **f** XRD patterns after electrochemical experiments; and **g** cycling stability and coulombic efficiency of NHPC-800 for 5000 cycles at 1 A g^{-1}

presented in Fig. 5b. The highly linear and relatively symmetric triangular curves can be clearly observed, implying typical electrical double-layer capacitance characteristic [59]. Obviously, NHPC-800 shows the highest specific capacitance of 251.4 F g^{-1} at 1 A g^{-1}, which is much better than NHPC-700 (134.8 F g^{-1}), NHPC-900 (162.7 F g^{-1}) and other source-prepared carbon materials (Table 2) [60–75]. This can be ascribed to two reasons as follows: (1) highly cross-linked porous morphology with plenty of micropores, mesopores and macropores is beneficial to effective aggrandizement of SSA and acceleration of ion transport and diffusion [40]; and (2) nitrogen doping is able to induce extra pseudocapacitance, improve conductivity and surface wettability of carbonaceous materials. For example, Hu et al. prepared N-doped reduced graphene oxide (N-RGO) and reduced graphene oxide (RGO) using microwave-assisted hydrothermal technique. The N-RGO possesses 3.0 at.% nitrogen content. It is found that the specific capacitances of N-RGO and RGO are 233.1 and 193.4 F g^{-1}, respectively [71]. Figure 5c shows the specific capacitances of specimens at various current density. Even at 10 A g^{-1}, NHPC-800 can still maintain at 203 F g^{-1} (80.7%), which can be attributed to its high SSA, well-developed pore structure and nitrogen-doping. The EIS from 10 mHz to 100 kHz is revealed in Fig. 5d. NHPC-*x* demonstrates nearly vertical linear parts at low frequency region, illustrating main electrical double layer charge storage behaviors [76]. Notably, NHPC-800 shows semicircular-like shape with smallest diameter at high frequency region (Fig. 5d), manifesting that NHPC-800 has excellent capacitive characteristic, superior conductivity and short ion diffusion route due to its high SSA, 3D interconnected porous morphology and nitrogen and oxygen functional groups. CV curve of NHPC-800 retains rectangle-like without palpable distortion even at 200 mV s^{-1} (Fig. 5e), suggesting remarkable rate property, which may be attributed to interrelated hierarchical porous morphology that provides abundant ion transport channels to promote ion diffusion [38]. Figure 5f shows the XRD patterns of NHPC-*x* after electrochemical test. The three intense peaks centered at 44.5°, 51.8° and 76.3° in all the three patterns are attributed to Ni foam substrate [77]. Diffraction peaks of amorphous carbon are nearly invisible, which may be attributed to its low mass loading (~4 mg). No other extra peaks are detected in all patterns, suggesting superior purity and stability of obtained specimens. The cyclic stability of NHPC-800 has been investigated by circulation measurement at 1 A g^{-1}. Besides, NHPC-800 has the specific capacitance retention as high as 99% after 5000 cycles (Fig. 5g), demonstrating superior cycling durability. Simultaneously, coulombic efficiency of NHPC-800 is 104.2%.

A symmetrical supercapacitor by using two pieces of NHPC-800 with the same size and weight was been assembled and tested in 6 M $EMIMBF_4$ electrolyte. In Fig. 6a, the CV curves of NHPC-800 at 5–200 mV s^{-1} under 0–3.5 V show quasi-rectangular shape, which indicates a great electrochemical capacitance behavior. As shown in Fig. 6b, NHPC-800 displays symmetrical triangular-like curves at 1–5 A g^{-1}, suggesting that NHPC-800 has a remarkable rate property and outstanding reversibility. Significantly, the capacitance of NHPC-800 can be calculated to be

Table 2 Supercapacitances performance of some reported carbon materials

Samples	Electrolyte	Scan rate	Capacitance (F g^{-1})	References
N-doped carbon spheres	KOH	0.5 A g^{-1}	213	[60]
Lignin (LHPC)	H_2SO_4	0.05 A g^{-1}	165	[61]
Enteromorpha (H700-2-1.5)	KOH	0.05 A g^{-1}	206	[62]
Auricularia (P-HT-A)	KOH	5 mV s^{-1}	196	[63]
Pomelo mesocarps	KOH	0.5 A g^{-1}	245	[64]
AC aerogel	H_2SO_4	0.125 A g^{-1}	251	[65]
PC	KOH	1 A g^{-1}	198	[66]
HPGM	KOH	0.1 A g^{-1}	238	[67]
carbon/GO	KOH	0.05 A g^{-1}	109	[68]
NG sheets	KOH	1 A g^{-1}	148	[69]
NG hydrogel	KOH	1 A g^{-1}	158	[70]
NG sheets	H_2SO_4	5 mV s^{-1}	218	[71]
NCs porous spheres	H_2SO_4	1 A g^{-1}	176	[72]
NCs networks	H_2SO_4	0.2 A g^{-1}	220	[73]
Porous NCs	H_2SO_4	5 mV s^{-1}	168	[74]
OMCs	KOH	0.1 A g^{-1}	200	[75]
Nitrogen-doped hierarchical porous carbon	KOH	1 A g^{-1}	251.4	This work

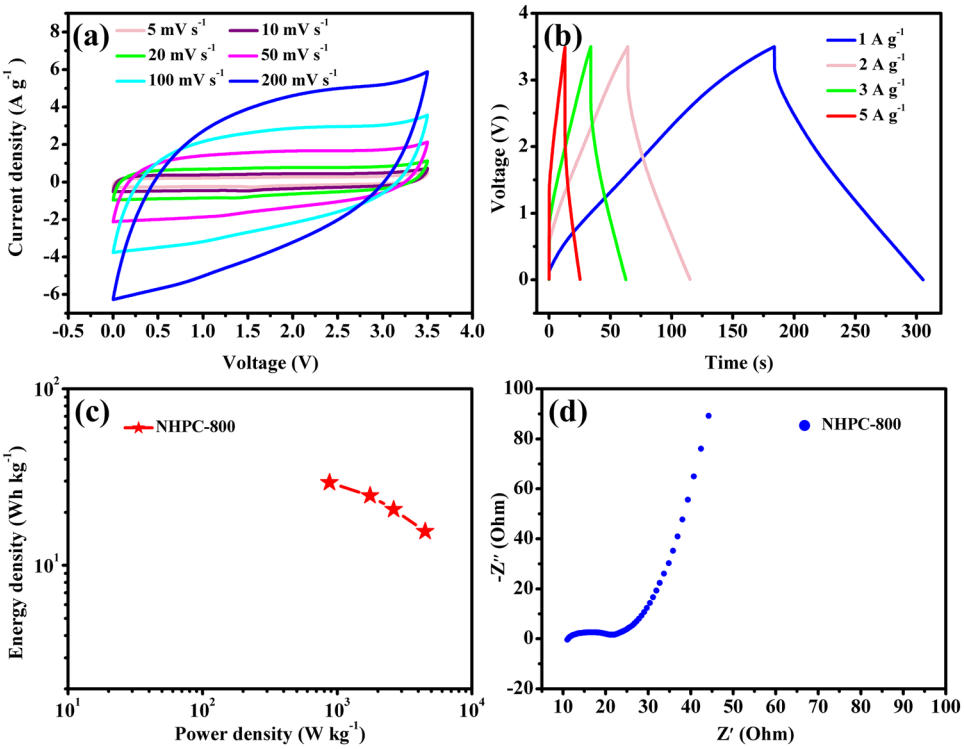

Fig. 6 Electrochemical property of NHPC-800 in two-electrode system in $EMIMBF_4$: **a** CV curves at 5–200 mV s^{-1}; **b** GCD curves at 1–5 A g^{-1}; **c** Ragone plot; and **d** Nyquist plot

69.92 F g^{-1} at 1 A g^{-1}. Besides, ragone plot of NHPC-800 is revealed in Fig. 6c. NHPC-800 exhibits an outstanding energy density of 29.43 Wh kg^{-1} at power density of 847.9 W kg^{-1}, and can still maintain 15.58 Wh kg^{-1} even at corresponding power density of 4497.83 W kg^{-1}, which is much better than some commercial carbonaceous materials [78, 79]. Figure 6d shows the Nyquist plot of NHPC-800. A vertical line in the low frequency region represents low transport and transfer resistance, implying typical electric double-layer capacitance behavior of NHPC-800. Meanwhile, there is a semicircle with small diameter in high-frequency region, which means a low charge-transfer resistance of carbon electrode.

4 Conclusion

The NHPC have been fabricated using pig nail as natural abundant protein-rich carbon source by the facile process of pre-carbonization and KOH high-temperature activation. Our results show that the micromorphology and structure can be effectively tailored by changing activation temperature. The optimum activation temperature is 800 °C at which the material has unique 3D honeycomb-like hierarchical porous morphology with ultrahigh SSA of 2563.30 m^2 g^{-1}, which are beneficial to rapid ion diffusion. Particularly, the existence of nitrogen functional groups is beneficial to introduce pseudocapacitance and increase conductivity and surface wettability. The specific capacity of NHPC-800 is 251.4 F g^{-1} at 1 A g^{-1} and cycling durability of NHPC-800 is still as high as 99% after 5000 cycles.

Acknowledgements This work was supported by Sichuan Science and Technology Program (2018JY0447).

References

1. J. Chang, Z. Gao, X. Wang, D. Wu, F. Xu, X. Wang, Y. Guo, K. Jiang, Activated porous carbon prepared from paulownia flower for high performance supercapacitor electrodes. Electrochim. Acta **157**, 290–298 (2015)
2. J. Yan, Q. Wang, T. Wei, Z. Fan, Recent advances in design and fabrication of electrochemical supercapacitors with high energy densities. Adv. Energy Mater. **4**(4), 1300816 (2014)
3. K. Srirangan, L. Akawi, M. Moo-Young, C.P. Chou, Towards sustainable production of clean energy carriers from biomass resources. Appl. Energy **100**, 172–186 (2012)
4. J.R. Miller, P. Simon, Materials science. Electrochemical capacitors for energy management. Science **321**(5889), 651–652 (2008)
5. Y. Wang, Y. Song, Y. Xia, Electrochemical capacitors: mechanism, materials, systems, characterization and applications. Chem. Soc. Rev. **45**(21), 5925–5950 (2016)
6. L.L. Zhang, X.S. Zhao, Carbon-based materials as supercapacitor electrodes. Chem. Soc. Rev. **38**(9), 2520–2531 (2009)
7. J. Yan, Z. Fan, W. Sun, G. Ning, T. Wei, Q. Zhang, R. Zhang, L. Zhi, F. Wei, Advanced asymmetric supercapacitors based on $Ni(OH)_2$/graphene and porous graphene electrodes with high energy density. Adv. Funct. Mater. **22**(12), 2632–2641 (2012)
8. L.Y. Chen, Y. Hou, J.L. Kang, A. Hirata, T. Fujita, M.W. Chen, Toward the theoretical capacitance of RuO_2 reinforced by highly conductive nanoporous gold. Adv. Energy Mater. **3**(7), 851–856 (2013)

9. Z.F. Li, H. Zhang, Q. Liu, L. Sun, L. Stanciu, J. Xie, Fabrication of high-surface-area graphene/polyaniline nanocomposites and their application in supercapacitors. ACS Appl. Mater. Interfaces **5**(7), 2685–2691 (2013)
10. L.-J. Xie, J.-F. Wu, C.-M. Chen, C.-M. Zhang, L. Wan, J.-L. Wang, Q.-Q. Kong, C.-X. Lv, K.-X. Li, G.-H. Sun, A novel asymmetric supercapacitor with an activated carbon cathode and a reduced graphene oxide–cobalt oxide nanocomposite anode. J. Power Sources **242**, 148–156 (2013)
11. T. Liu, L. Finn, M. Yu, H. Wang, T. Zhai, X. Lu, Y. Tong, Y. Li, Polyaniline and polypyrrole pseudocapacitor electrodes with excellent cycling stability. Nano Lett. **14**(5), 2522–2527 (2014)
12. C. Zhou, Y. Zhang, Y. Li, J. Liu, Construction of high-capacitance 3D CoO@polypyrrole nanowire array electrode for aqueous asymmetric supercapacitor. Nano Lett. **13**(5), 2078–2085 (2013)
13. Q. Lu, Y. Zhou, Synthesis of mesoporous polythiophene/MnO_2 nanocomposite and its enhanced pseudocapacitive properties. J. Power Sources **196**(8), 4088–4094 (2011)
14. Z. Lei, Z. Liu, H. Wang, X. Sun, L. Lu, X.S. Zhao, A high-energy-density supercapacitor with graphene–CMK-5 as the electrode and ionic liquid as the electrolyte. J. Mater. Chem. A **1**(6), 2313 (2013)
15. F. Miao, C. Shao, X. Li, K. Wang, N. Lu, Y. Liu, Electrospun carbon nanofibers/carbon nanotubes/polyaniline ternary composites with enhanced electrochemical performance for flexible solid-state supercapacitors. ACS Sustain. Chem. Eng. **4**(3), 1689–1696 (2016)
16. X. He, H. Zhang, H. Zhang, X. Li, N. Xiao, J. Qiu, Direct synthesis of 3D hollow porous graphene balls from coal tar pitch for high performance supercapacitors. J. Mater. Chem. A **2**(46), 19633–19640 (2014)
17. L. Hao, X. Li, L. Zhi, Carbonaceous electrode materials for supercapacitors. Adv. Mater. **25**(28), 3899–3904 (2013)
18. D.S. Su, R. Schlogl, Nanostructured carbon and carbon nanocomposites for electrochemical energy storage applications. ChemSusChem **3**(2), 136–168 (2010)
19. P. Trogadas, T.F. Fuller, P. Strasser, Carbon as catalyst and support for electrochemical energy conversion. Carbon **75**, 5–42 (2014)
20. C.-Y. Li, J. Patra, C.-H. Yang, C.-M. Tseng, S.B. Majumder, Q.-F. Dong, J.-K. Chang, Electrolyte optimization for enhancing electrochemical performance of antimony sulfide/graphene anodes for sodium-ion batteries–carbonate-based and ionic liquid electrolytes. ACS Sustain. Chem. Eng. **5**(9), 8269–8276 (2017)
21. Y. Zhou, J. Ren, L. Xia, H. Wu, F. Xie, Q. Zheng, C. Xu, D. Lin, Nitrogen-doped hierarchical porous carbon framework derived from waste pig nails for high-performance supercapacitors. ChemElectroChem **4**(12), 3181–3187 (2017)
22. M. Biswal, A. Banerjee, M. Deo, S. Ogale, From dead leaves to high energy density supercapacitors. Energy Environ. Sci. **6**(4), 1249 (2013)
23. H.-J. Liu, J. Wang, C.-X. Wang, Y.-Y. Xia, Ordered hierarchical mesoporous/microporous carbon derived from mesoporous titanium-carbide/carbon composites and its electrochemical performance in supercapacitor. Adv. Energy Mater. **1**(6), 1101–1108 (2011)
24. H. Zhou, S. Zhu, M. Hibino, I. Honma, Electrochemical capacitance of self-ordered mesoporous carbon. J. Power Sources **122**(2), 219–223 (2003)
25. Y. Li, Z. Li, P.K. Shen, Simultaneous formation of ultrahigh surface area and three-dimensional hierarchical porous graphene-like networks for fast and highly stable supercapacitors. Adv. Mater. **25**(17), 2474–2480 (2013)
26. S.L. Candelaria, B.B. Garcia, D. Liu, G. Cao, Nitrogen modification of highly porous carbon for improved supercapacitor performance. J. Mater. Chem. **22**(19), 9884 (2012)
27. Y. Zhai, Y. Dou, D. Zhao, P.F. Fulvio, R.T. Mayes, S. Dai, Carbon materials for chemical capacitive energy storage. Adv. Mater. **23**(42), 4828–4850 (2011)
28. M. Zhou, F. Pu, Z. Wang, S. Guan, Nitrogen-doped porous carbons through KOH activation with superior performance in supercapacitors. Carbon **68**, 185–194 (2014)
29. B. Qiu, C. Pan, W. Qian, Y. Peng, L. Qiu, F. Yan, Nitrogen-doped mesoporous carbons originated from ionic liquids as electrode materials for supercapacitors. J. Mater. Chem. A **1**(21), 6373 (2013)
30. Z. Li, Z. Xu, H. Wang, J. Ding, B. Zahiri, C.M.B. Holt, X. Tan, D. Mitlin, Colossal pseudocapacitance in a high functionality–high surface area carbon anode doubles the energy of an asymmetric supercapacitor. Energy Environ. Sci. **7**(5), 1708–1718 (2014)
31. L.-F. Chen, Z.-H. Huang, H.-W. Liang, W.-T. Yao, Z.-Y. Yu, S.-H. Yu, Flexible all-solid-state high-power supercapacitor fabricated with nitrogen-doped carbon nanofiber electrode material derived from bacterial cellulose. Energy Environ. Sci. **6**(11), 3331 (2013)
32. F. Gao, G. Shao, J. Qu, S. Lv, Y. Li, M. Wu, Tailoring of porous and nitrogen-rich carbons derived from hydrochar for high-performance supercapacitor electrodes. Electrochim. Acta **155**, 201–208 (2015)
33. Y.-H. Lin, T.-Y. Wei, H.-C. Chien, S.-Y. Lu, Manganese oxide/carbon aerogel composite: an outstanding supercapacitor electrode material. Adv. Energy Mater. **1**(5), 901–907 (2011)
34. Z.J. Qiao, M.M. Chen, C.Y. Wang, Y.C. Yuan, Humic acids-based hierarchical porous carbons as high-rate performance electrodes for symmetric supercapacitors. Bioresour. Technol. **163**, 386–389 (2014)
35. W. Qian, F. Sun, Y. Xu, L. Qiu, C. Liu, S. Wang, F. Yan, Human hair-derived carbon flakes for electrochemical supercapacitors. Energy Environ. Sci. **7**(1), 379–386 (2014)
36. Y. Wang, R. Yang, Y. Wei, Z. Zhao, M. Li, Preparation of novel pigskin-derived carbon sheets and their low-temperature activation-induced high capacitive performance. RSC Adv. **4**(85), 45318–45324 (2014)
37. X. Wu, L. Jiang, C. Long, Z. Fan, From flour to honeycomb-like carbon foam: carbon makes room for high energy density supercapacitors. Nano Energy **13**, 527–536 (2015)
38. L. Sun, C. Tian, M. Li, X. Meng, L. Wang, R. Wang, J. Yin, H. Fu, From coconut shell to porous graphene-like nanosheets for high-power supercapacitors. J. Mater. Chem. A **1**(21), 6462 (2013)
39. N. Guo, M. Li, X. Sun, F. Wang, R. Yang, Enzymatic hydrolysis lignin derived hierarchical porous carbon for supercapacitors in ionic liquids with high power and energy densities. Green Chem. **19**(11), 2595–2602 (2017)
40. J. Ding, H. Wang, Z. Li, K. Cui, D. Karpuzov, X. Tan, A. Kohandehghan, D. Mitlin, Peanut shell hybrid sodium ion capacitor with extreme energy–power rivals lithium ion capacitors. Energy Environ. Sci. **8**(3), 941–955 (2015)
41. D. Hulicova-Jurcakova, M. Seredych, G.Q. Lu, T.J. Bandosz, Combined effect of nitrogen- and oxygen-containing functional groups of microporous activated carbon on its electrochemical performance in supercapacitors. Adv. Funct. Mater. **19**(3), 438–447 (2009)
42. H. Wu, Y. Deng, J. Mou, Q. Zheng, F. Xie, E. Long, C. Xu, D. Lin, Activator-induced tuning of micromorphology and electrochemical properties in biomass carbonaceous materials derived from mushroom for lithium-sulfur batteries. Electrochim. Acta **242**, 146–158 (2017)
43. A.M. Abioye, F.N. Ani, Recent development in the production of activated carbon electrodes from agricultural waste biomass for supercapacitors: a review. Renew. Sustain. Energy Rev. **52**, 1282–1293 (2015)
44. Q. Wang, Q. Cao, X. Wang, B. Jing, H. Kuang, L. Zhou, A high-capacity carbon prepared from renewable chicken feather

biopolymer for supercapacitors. J. Power Sources **225**, 101–107 (2013)
45. M. Armandi, B. Bonelli, F. Geobaldo, E. Garrone, Nanoporous carbon materials obtained by sucrose carbonization in the presence of KOH. Microporous Mesoporous Mater. **132**(3), 414–420 (2010)
46. M.M. Wan, X.D. Sun, Y.Y. Li, J. Zhou, Y. Wang, J.H. Zhu, Facilely fabricating multifunctional N-enriched carbon. ACS Appl. Mater. Interfaces **8**(2), 1252–1263 (2016)
47. J. Guo, H. Guo, L. Zhang, B. Yang, J. Cui, Hierarchically porous carbon as a high-rate and long-life electrode material for high-performance supercapacitors. ChemElectroChem **5**(5), 770–777 (2018)
48. X.Y. Chen, C. Chen, Z.J. Zhang, D.H. Xie, X. Deng, J.W. Liu, Nitrogen-doped porous carbon for supercapacitor with long-term electrochemical stability. J. Power Sources **230**, 50–58 (2013)
49. X. Liu, D. Chao, Y. Li, J. Hao, X. Liu, J. Zhao, J. Lin, H. Jin Fan, Z. Xiang Shen, A low-cost and one-step synthesis of N-doped monolithic quasi-graphene films with porous carbon frameworks for Li-ion batteries. Nano Energy **17**, 43–51 (2015)
50. B. Duan, X. Gao, X. Yao, Y. Fang, L. Huang, J. Zhou, L. Zhang, Unique elastic N-doped carbon nanofibrous microspheres with hierarchical porosity derived from renewable chitin for high rate supercapacitors. Nano Energy **27**, 482–491 (2016)
51. D. Usachov, O. Vilkov, A. Gruneis, D. Haberer, A. Fedorov, V.K. Adamchuk, A.B. Preobrajenski, P. Dudin, A. Barinov, M. Oehzelt, C. Laubschat, D.V. Vyalikh, Nitrogen-doped graphene: efficient growth, structure, and electronic properties. Nano Lett. **11**(12), 5401–5407 (2011)
52. J. Li, S. Wang, Y. Ren, Z. Ren, Y. Qiu, J. Yu, Nitrogen-doped activated carbon with micrometer-scale channels derived from luffa sponge fibers as electrocatalysts for oxygen reduction reaction with high stability in acidic media. Electrochim. Acta **149**, 56–64 (2014)
53. B. Xu, S. Hou, G. Cao, F. Wu, Y. Yang, Sustainable nitrogen-doped porous carbon with high surface areas prepared from gelatin for supercapacitors. J. Mater. Chem. **22**(36), 19088 (2012)
54. Y. Li, G. Wang, T. Wei, Z. Fan, P. Yan, Nitrogen and sulfur co-doped porous carbon nanosheets derived from willow catkin for supercapacitors. Nano Energy **19**, 165–175 (2016)
55. Z. Li, L. Zhang, B.S. Amirkhiz, X. Tan, Z. Xu, H. Wang, B.C. Olsen, C.M.B. Holt, D. Mitlin, Carbonized chicken eggshell membranes with 3D architectures as high-performance electrode materials for supercapacitors. Adv. Energy Mater. **2**(4), 431–437 (2012)
56. C. Zhang, X. Zhu, M. Cao, M. Li, N. Li, L. Lai, J. Zhu, D. Wei, Hierarchical porous carbon materials derived from sheep manure for high-capacity supercapacitors. ChemSusChem **9**(9), 932–937 (2016)
57. A. Alabadi, X. Yang, Z. Dong, Z. Li, B. Tan, Nitrogen-doped activated carbons derived from a co-polymer for high supercapacitor performance. J. Mater. Chem. A **2**(30), 11697–11705 (2014)
58. J. Qu, C. Geng, S. Lv, G. Shao, S. Ma, M. Wu, Nitrogen, oxygen and phosphorus decorated porous carbons derived from shrimp shells for supercapacitors. Electrochim. Acta **176**, 982–988 (2015)
59. L. Sun, C. Tian, Y. Fu, Y. Yang, J. Yin, L. Wang, H. Fu, Nitrogen-doped porous graphitic carbon as an excellent electrode material for advanced supercapacitors. Chemistry **20**(2), 564–574 (2014)
60. J. Han, G. Xu, B. Ding, J. Pan, H. Dou, D.R. MacFarlane, Porous nitrogen-doped hollow carbon spheres derived from polyaniline for high performance supercapacitors. J. Mater. Chem. A **2**(15), 5352–5357 (2014)
61. W. Zhang, H. Lin, Z. Lin, J. Yin, H. Lu, D. Liu, M. Zhao, 3 D hierarchical porous carbon for supercapacitors prepared from lignin through a facile template-free method. ChemSusChem **8**(12), 2114–2122 (2015)
62. M. Wu, P. Li, Y. Li, J. Liu, Y. Wang, Enteromorpha based porous carbons activated by zinc chloride for supercapacitors with high capacity retention. RSC Adv. **5**(21), 16575–16581 (2015)
63. H. Zhu, X. Wang, F. Yang, X. Yang, Promising carbons for supercapacitors derived from fungi. Adv. Mater. **23**(24), 2745–2748 (2011)
64. H. Peng, G. Ma, K. Sun, Z. Zhang, Q. Yang, Z. Lei, Nitrogen-doped interconnected carbon nanosheets from pomelo mesocarps for high performance supercapacitors. Electrochim. Acta **190**, 862–871 (2016)
65. Z. Zapata-Benabithe, F. Carrasco-Marin, J. de Vicente, C. Moreno-Castilla, Carbon xerogel microspheres and monoliths from resorcinol-formaldehyde mixtures with varying dilution ratios: preparation, surface characteristics, and electrochemical double-layer capacitances. Langmuir. **29**(20), 6166–6173 (2013)
66. E. Raymundo-Piñero, F. Leroux, F. Béguin, A high-performance carbon for supercapacitors obtained by carbonization of a seaweed biopolymer. Adv. Mater. **18**(14), 1877–1882 (2006)
67. Y. Tao, X. Xie, W. Lv, D.M. Tang, D. Kong, Z. Huang, H. Nishihara, T. Ishii, B. Li, D. Golberg, F. Kang, T. Kyotani, Q.H. Yang, Towards ultrahigh volumetric capacitance: graphene derived highly dense but porous carbons for supercapacitors. Sci. Rep. **3**, 2975 (2013)
68. M. Seredych, T.J. Bandosz, S-doped micro/mesoporous carbon–graphene composites as efficient supercapacitors in alkaline media. J. Mater. Chem. A **1**(38), 11717 (2013)
69. J.W. Lee, J.M. Ko, J.-D. Kim, Hydrothermal preparation of nitrogen-doped graphene sheets via hexamethylenetetramine for application as supercapacitor electrodes. Electrochim. Acta **85**, 459–466 (2012)
70. P. Chen, J.-J. Yang, S.-S. Li, Z. Wang, T.-Y. Xiao, Y.-H. Qian, S.-H. Yu, Hydrothermal synthesis of macroscopic nitrogen-doped graphene hydrogels for ultrafast supercapacitor. Nano Energy **2**(2), 249–256 (2013)
71. Y.-H. Lee, K.-H. Chang, C.-C. Hu, Differentiate the pseudocapacitance and double-layer capacitance contributions for nitrogen-doped reduced graphene oxide in acidic and alkaline electrolytes. J. Power Sources **227**, 300–308 (2013)
72. C. Shen, Y. Sun, W. Yao, Y. Lu, Facile synthesis of polypyrrole nanospheres and their carbonized products for potential application in high-performance supercapacitors. Polymer **55**(12), 2817–2824 (2014)
73. L. Hao, B. Luo, X. Li, M. Jin, Y. Fang, Z. Tang, Y. Jia, M. Liang, A. Thomas, J. Yang, L. Zhi, Terephthalonitrile-derived nitrogen-rich networks for high performance supercapacitors. Energy Environ. Sci. **5**(12), 9747 (2012)
74. S. Wang, C. Han, J. Wang, J. Deng, M. Zhu, J. Yao, H. Li, Y. Wang, Controlled synthesis of ordered mesoporous carbohydrate-derived carbons with flower-like structure and N-doping by self-transformation. Chem. Mater. **26**(23), 6872–6877 (2014)
75. Q. Wang, W. Xia, W. Guo, L. An, D. Xia, R. Zou, Functional zeolitic-imidazolate-framework-templated porous carbon materials for CO_2 capture and enhanced capacitors. Chem. Asian J. **8**(8), 1879–1885 (2013)
76. L. Qie, W. Chen, H. Xu, X. Xiong, Y. Jiang, F. Zou, X. Hu, Y. Xin, Z. Zhang, Y. Huang, Synthesis of functionalized 3D hierarchical porous carbon for high-performance supercapacitors. Energy Environ. Sci. **6**(8), 2497 (2013)
77. S. Chandra Sekhar, G. Nagaraju, J.S. Yu, High-performance pouch-type hybrid supercapacitor based on hierarchical NiO–Co_3O_4–NiO composite nanoarchitectures as an advanced electrode material. Nano Energy **48**, 81–92 (2018)
78. H. Wu, Y. Li, J. Ren, D. Rao, Q. Zheng, L. Zhou, D. Lin, CNT-assembled dodecahedra core@nickel hydroxide nanosheet shell enabled sulfur cathode for high-performance lithium-sulfur batteries. Nano Energy **55**, 82–92 (2019)
79. R. Raccichini, A. Varzi, S. Passerini, B. Scrosati, The role of graphene for electrochemical energy storage. Nat. Mater. **14**(3), 271–279 (2015)